ASTRONOMY & ASTROPHYSICS
SUPPLEMENT SERIES

JANUARY I **1999**, PAGE 75

Astron. Astrophys. Suppl. Ser. **134**, 75–86 (1999)

The central region of the Fornax cluster

II. Spectroscopy and radial velocities of member and background galaxies

M. Hilker[1,2], L. Infante[2], G. Vieira[2], M. Kissler-Patig[1,3,4], and T. Richtler[1]

[1] Sternwarte der Universität Bonn, Auf dem Hügel 71, 53121 Bonn, Germany
[2] Departamento de Astronomía y Astrofísica, P. Universidad Católica, Casilla 104, Santiago 22, Chile
[3] UCO/Lick Observatory, University of California, Santa Cruz, CA 95064, U.S.A.
[4] Feodor Lynen Fellow of the Alexander von Humboldt Foundation

Received March 23; accepted July 7, 1998

Abstract. Radial velocities of 94 galaxies brighter than about $V_{\rm tot} = 20$ mag in the direction of the central Fornax cluster have been measured[1]. Except for 8 Fornax members, all galaxies lie in the background. Among the 8 members, there are 5 nucleated dwarf ellipticals that are already listed in the FCC (Ferguson 1989). Two of the 3 "new" members are very compact and have surface brightnesses comparable to globular clusters, however their luminosities are in the range of dwarf elliptical nuclei.

The measured line indices (especially Mg2, Hβ, and iron) of the brighter of the compact objects suggest a solar metallicity, whereas the fainter compact object as well as the dE, Ns have line indices that are similar to those of old metal-poor globular clusters (GCs). However, with these data it is not possible to clearly classify the compact objects either as very bright globular clusters, isolated nuclei of dE, Ns, or even compact ellipticals.

A background galaxy cluster at $z = 0.11$ has been found just behind the center of the Fornax cluster. This explains the excess population of galaxies reported in Paper I. The brightest galaxy of the background cluster lies only 1.′1 south of NGC 1399 and is comparable in absolute luminosity with the central Fornax galaxy itself.

Key words: galaxies: clusters: Fornax cluster — galaxies: distances and redshifts — galaxies: abundances — galaxies: dwarf

Send offprint requests to: M. Hilker

[1] Table 2 containing the position, magnitude and velocity of all galaxies is also available in electronic form at the CDS via anonymous ftp to cdsarc.u-strasbg.fr (130.79.128.5) or via http://cdsweb.u-strasbg.fr/Abstract.html

1. Introduction

In the center of galaxy clusters the various types of dwarf galaxies differ in properties, such as their spatial distribution and luminosity function. Early-type dwarf ellipticals, especially nucleated ones, are the most clustered, whereas late-type dwarfs are preferentially found at the outskirts of clusters (e.g. review by Ferguson & Binggeli 1994, and references therein). The different environmental properties probably reflect the result of the dynamical procresses during the formation and evolution epoch of the clusters.

Among low mass galaxies, a striking but rare subgroup are the compact ellipticals (cEs), or M 32-type galaxies. It is under discussion, whether environmental effects such as tidal stripping have shaped their present appearance (e.g. Faber 1973) or whether these galaxies just represent the low-luminosity end of the giant ellipticals (Nieto & Prugniel 1987). E.g., M 32 itself is a companion of the Andromeda galaxy (M 31). The non-existence of any globular cluster (GC) in this galaxy suggests that previously present GCs might have been captured by M 31 during past close passages. Whether the interaction with M 31 also has formed the compact shape of M 32 remains unclear.

At the distance of the nearest galaxy clusters, the classification of compact objects such as M 32 just by morphological properties is nearly impossible. Their high central surface brightness and de Vaucouleurs surface brightness profile make them indistinguishable from background ellipticals. In the Fornax Cluster Catalog (FCC) of possible members and likely background galaxies, Ferguson (1989) lists 131 candidate cEs. Recently, Drinkwater et al. (1997, see also Drinkwater & Gregg 1998) have measured radial velocities of 67 of them. No one is member of the Fornax cluster. The fact that very few cEs are found indicates that tidal stripping does not play a major role in their formation in rich environments. However, the member and

background galaxy catalogs of Ferguson are limited in the angular diameter of the objects. Especially, galaxies with diameters comparable to M 32 itself and smaller compact ellipticals are beyond the resolution limit of Ferguson's sample.

A second type of objects in the galaxy cluster populations that could easily be missed by morphological classifications are nuclei of tidally disrupted nucleated dwarf ellipticals (dE, Ns). Numerical simulations by Bassino et al. (1994) reveal that such nuclei can survive the dissolution in the gravitational field even during the entire lifetime of the universe and would appear as luminous globular cluster-like objects. The nuclear magnitudes of all Virgo dE, Ns (Binggeli & Cameron 1991), for example, fall indeed in the magnitude – surface brightness sequence defined by the globular clusters (e.g. Binggeli 1994). At the distance of the Fornax cluster, these objects would hardly be resolved and can only be uncovered by spectroscopic observations.

In the first paper (Hilker et al. 1998, hereafter Paper I) a galaxy catalog with photometric properties and surface brightness profiles for galaxies in selected fields of the central Fornax cluster has been presented. An excess population of galaxies near NGC 1399, the central galaxy of the cluster, has been found as compared to the other Fornax fields and to absolute background fields. The photometric analysis has shown that most of the excess galaxies have sizes and surface brightnesses which are more typical for background spirals and ellipticals than for dwarf ellipticals. However, as discussed before, photometric properties alone are not sufficient to distinguish between background galaxies and high surface brightness dwarf galaxies in the Fornax cluster. This paper presents redshift determinations of a bright sub-sample of our photometric catalog (Paper I) to investigate the nature of the mentioned excess galaxies. Furthermore, line indices for the objects that have been identified as Fornax members were measured.

In the following the expression "radial velocity" has been used for the measurement of cz instead of redshift, being aware of the fact that the true radial velocity for high z differs from cz depending on the applied cosmological model.

Previous radial velocity measurements of galaxies in the Fornax cluster brighter than $B_{\rm T} = 15.5$ mag were presented by Jones & Jones (1980), Lauberts (1982) and Richter & Sadler (1985). They are compiled in the Fornax Cluster Catalog (FCC) by Ferguson (1989). Except for the giant galaxies, there are only two galaxies that overlap with our sample: NGC 1396 and FCC 222, two bright dE, Ns. Held & Mould (1994) took spectra of 10 dE, Ns in the Fornax cluster; one of these is in common with our sample.

Sections 2, 3, and 4 give a detailed description of the observations, data reduction, and velocity determination. The resulting radial velocities and the analysis of individual objects are presented in Sect. 5. The main results are summarized in Sect. 6.

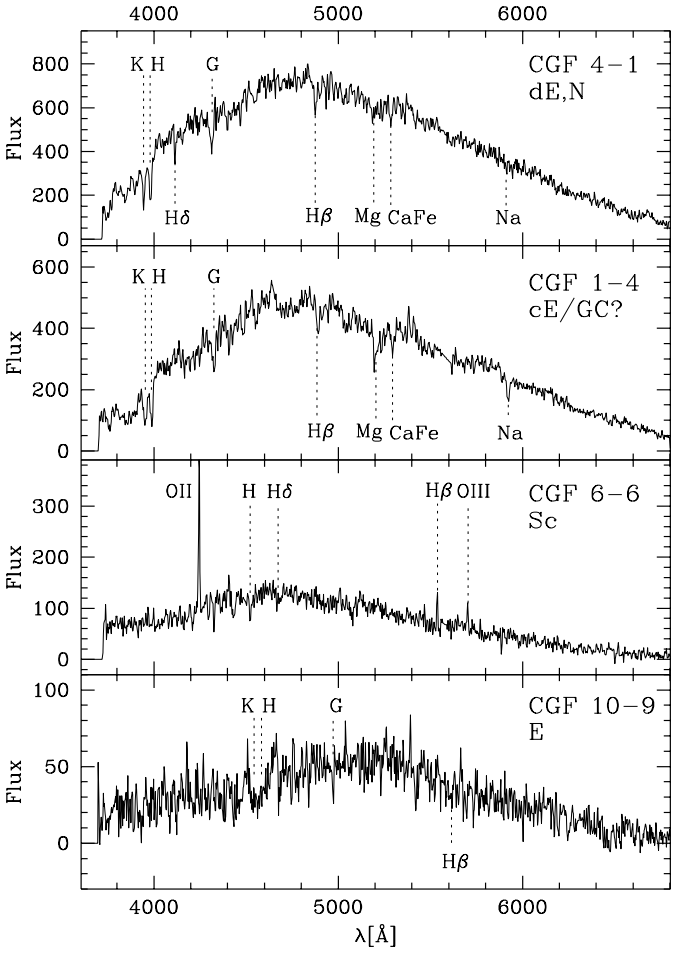

Fig. 1. Typical spectra after subtraction of the sky spectra. The uppermost panel shows the nucleated dwarf elliptical NGC 1396. In the panel below the spectrum of the compact nucleus-like Fornax member CGF 1-4 is shown. In the third panel a typical emission line spectrum of a background spiral is plotted. The spectrum in the bottom panel has a signal-to-noise at the limit where velocity measurements are still feasible

2. Observations

The observations have been performed with the 2.5 m DuPont telescope at the Las Campanas Observatory, Chile, during the nights of 7–9 December, 1996. The multi-fiber spectrograph from Shectman (1989) has been used. The field of view is 1.5×1.5 degree. The aperture size of each fiber is 2 arcsec in diameter on the sky. The fibers were connected with a Boller & Chivens spectrograph coupled to a 2DFrutti detector (2DF). With a blaze angle of $9°45'$ we got a spectral range of 3800 Å − 6800 Å. The spectra are projected to a 1520×1024 pixel area, with a dispersion of $\simeq 2 - 3$ Å· pixel^{-1} and a final resolution of $\simeq$5 Å.

From our catalog 125 galaxies brighter than $V = 20.0$ mag were selected. Accurate positions have been obtained by using reference stars from the Guide Star Catalog. Astrometric solutions yielded positions with accuracies better than $0\farcs3$. In addition, three bright dE, Ns have been included from the FCC (Ferguson 1989), namely FCC 188, FCC 222, and FCC 274. Their positions are not as accurate as those of the CCD sample. Small positional deviations for these objects resulted in quite low signal-to-noise spectra despite the high central surface brightnesses of their nuclei. The whole sample was divided in two sets of positions in order to avoid overlaps in the fiber configuration. In spite of this, 13 positions could not be taken. About 20 to 30 fibers per set were positioned as sky fibers to random positions in the field. The integration times of the first and second set were 4 hours and 4.5 hours respectively. For the wavelength calibration comparison HeNe spectra have been obtained at the two positions before and after the long integrations. Additionally, long flatfield exposures have been taken. We have chosen different grating angles between $8°45'$ and $10°45'$ to get an homogenous illumination of the whole spectral range.

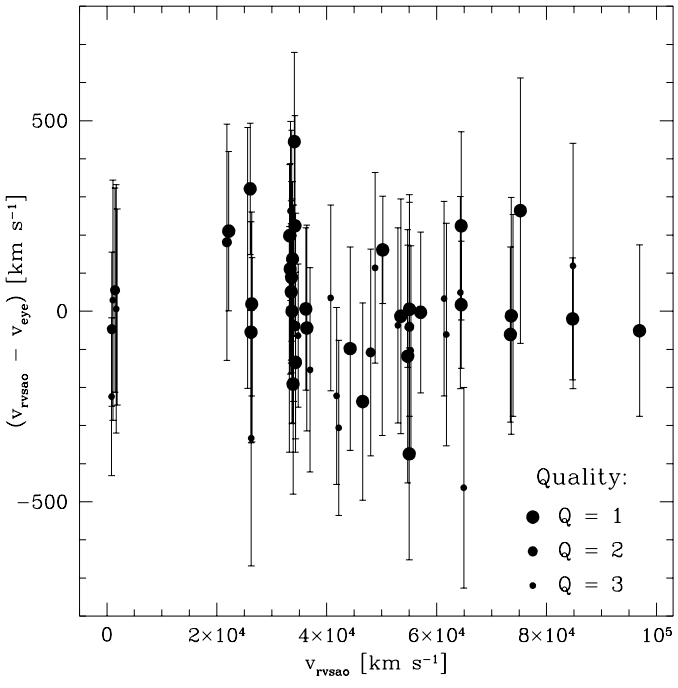

Fig. 2. This plot shows the differences of the two independent methods of velocity determinations. The rms error of the scatter of the most reliable identifications ($Q = 1$ and 2) is about 150 km s^{-1}

3. Reductions

All reduction steps have been performed with packages under IRAF. We followed essentially the method described by Way et al. (1998) with the following basic reductions steps.

All spectra are arranged side by side on the 2DF $x-y$-pixel image, the y direction being the direction of dispersion. Since the spectra have a strong curvature on the $x-y$-pixel plane, they have to be straightened first. We fitted a transformation of the plane in x direction by tracing the features in the combined image of the flatfield exposures. Similarily, the features in the combined calibration lamp exposure were fitted for the y transformation. All images were straightened by these two transformations. (This procedure uses the IRAF tasks *identify, reidentify, fitcoords* and *transform* in the *noao.twodspec.longslit* package.)

The extraction of the single spectra, tracing of the apertures, fitting of the flatfield, wavelength calibration with the two arc spectra, and subtraction of the sky spectra have been done with the *dohydra* package. The residual sky lines in the spectra were cleaned with the *lineclean* task. The typical rms error of the solution for the wavelength calibration is less than 0.3 Å.

Figure 1 shows 4 typical spectra of different signal-to-noise, with some reference lines indicated.

4. Radial velocity measurements

The radial velocities cz have been determined by two different, independent methods: first, "automatic" identification of the absorption and/or emission lines and fourier cross correlation with template spectra using the *rvsao* package; second, "by eye" identification of absorption lines and computation of cz with the task *rvidlines*. Both methods were applied to all measured spectra.

A number of our spectra show O II, Hβ, and O III in emission. Emission lines were removed from the spectra and a cross-correlation analysis was carried out. Radial velocities were also independently measured for these emission lines.

For the first method high signal-to-noise spectra of selected galaxies (NGC 1407, NGC 1426, and NGC 1700) were employed as templates in the the cross-correlation analysis. These templates were observed with the same instrument. A synthetic spectrum, as in Way et al. (1998), was also used. All templates were rebinned to the same resolution as the fiber spectra and were corrected for heliocentric velocity. The task *xcsao* crosscorrelates the emission-line-cleaned object spectra with the template spectra and generates a reliability factor called the R value which depends on the amplitude of the cross correlation peak. A low R value ($R < 4$) indicates that one should control the results by eye. The "best" velocity, as judged by the highest R value was adopted. In cases where strong emission lines, especially the O II line, were present we

Table 1. Objects whose spectra have a dominant contribution by light of a close Fornax giant galaxy

Object id.	giant NGC	light ratio	$v_{\rm giant}$ [km s^{-1}]	Q	$v_{\rm obj}$ [km s^{-1}]	Q
CGF 9-9	1374	0.79	1414 ± 71	2	38490 ± 74	3
CGF 8-3	1379	7.33	1504 ± 49	1		
CGF 6-5	1387	1.65	1277 ± 38	1		
CGF 3-11	1399	1.62	1541 ± 57	3	34225 ± 70	1
CGF 4-5	1399	4.00	1443 ± 45	1		
CGF 4-8	1399	0.26	1281 ± 97	2	33531 ± 52	2
CGF 1-13	1404	0.02	2253 ± 85	4	44267 ± 105	4
CGF 10-1	1427	1.01	1349 ± 40	1	16409 ± 40	2
CGF 10-14	1427	1.28	1483 ± 48	1		

calculated in addition their velocities with the task (*emsao*). In some cases where the absorption lines were very weak, but the emission lines clearly visible, the estimated emission line velocity could be used to improve the absorption line detection with *xcsao*. The absorption line velocities $v_{\rm cross}$ as well as the emission line velocities $v_{\rm em}$ are presented in Table 2.

The second method is based on the following steps: the Balmer jump and the close K and/or H lines were identified by eye and marked for the IRAF task *rvidlines* which compares the marked lines with a list of absorption lines. All identified lines with a sufficient signal-to-noise were used for the velocity calculation. The centering algorithm used for the position of the lines calculates the wavelength where the total flux of the absorption feature is divided into equal halfs. The resulting velocities $v_{\rm rvid}$ are presented in Table 2.

The results of both methods were compared. In 18 of the 115 spectra the signal-to-noise was too low to determine a velocity by either of the methods. In 68 spectra the velocities of both methods agree within ±500 km s^{-1}. Figure 2 shows the differences of the two determinations. The standard deviation is about 130 km s^{-1}, comparable to the rms errors of the fit to individual velocity determinations. One of our galaxies, the nucleated dwarf elliptical NGC 1396, was measured in both fiber sets. The signal-to-noise is one of the highest in our sample. The velocities of the "automatic" identification agree very well: 865 ± 17 and 871 ± 32 km s^{-1}. The "by eye" identification yields 870 ± 44 and 918 ± 52 km s^{-1}. Within the errors all values are consistent and agree with the published value by Jones & Jones (1980): 894 ± 120 km s^{-1}.

In 9 cases where the object is located very close to a Fornax elliptical or S0 galaxy, most probably the light, and thus the velocity of the giant was measured instead that of the object. In 5 of these spectra a second velocity was found indeed. In Table 1 we give the name of the Fornax galaxy, the ratio of the Fornax giant galaxy to target object light in a 2 arcsec aperture, the velocity of both components, and the identification quality as defined in the next section.

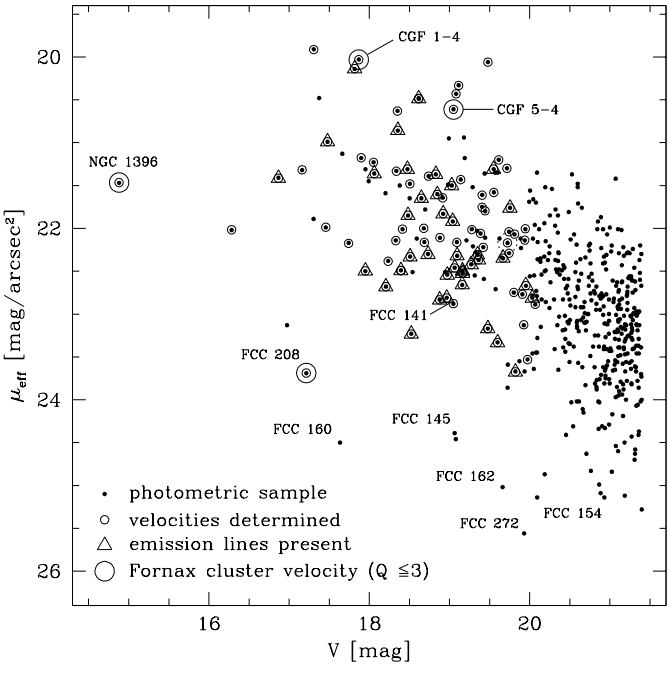

Fig. 3. In this magnitude – surface brightness diagram all galaxies of our photometric sample brighter than $V = 21.5$ mag are plotted. Galaxies with velocity determinations are encircled with small circles. The background galaxies that show emission lines are indicated with triangles. Only the galaxies encircled with large circles are Fornax members. The spectra of most dwarf galaxies have a too low signal-to-noise for line identifications. Note that the dE, Ns FCC 188, FCC 222, and FCC 274 are not plotted, since they do not belong to our photometric sample

5. Results

94 radial velocities were measured (not including the velocities of the giant galaxies of Table 1). The data are listed in Table 2 in order of increasing right ascension. The first column is the catalog name from Paper I. Column 2 gives the galaxy type as determined by morphological appearance, surface brightness profile (see Paper I), and spectral type. For the spectral classification the spectrophotometric atlas of galaxies by Kennicutt (1992) was used for comparison. Columns 3 – 5 are the right ascension, declination (epoch 2000.0) and total V magnitude from Paper I. Columns 6 – 9 are the heliocentric velocity of the cross correlation technique $v_{\rm cross}$, the R value, the velocity of the second determination method $v_{\rm rvid}$, and the emission line velocity $v_{\rm em}$, if available. In Cols. 10 and 11 the final adopted velocity and a mean error of the different determinations are given. In most of the cases, the final velocity is the mean of $v_{\rm cross}$ and $v_{\rm rvid}$. In the cases where the emission line velocity is based on at least 2 clearly

Table 2. Radial velocities of galaxies in and behind the Fornax cluster

Object Id.	Type	RA(2000)	Dec(2000)	V	$v_{\rm cross}$	R	$v_{\rm rvid}$	$v_{\rm em}$	$v_{\rm helio}$	error$_v$	Q
CGF 9-5	S/BCD?	3:34:57.23	−35:12:24.7	19.06				16833	16833	95	3
CGF 9-2	S	3:34:59.79	−35:09:58.1	18.24			18649	18058	18354	77	4
CGF 9-3a	Sc/I?	3:35:02.47	−35:11:49.6	18.39	10939	4.5	10396		10649	63	3
CGF 9-3b	Sc/I?	3:35:02.47	−35:11:49.6	18.39				21205	21205	75	3
CGF 9-7	E	3:35:06.52	−35:10:54.1	19.28	61733	5.0	61794		61763	61	1
CGF 9-9	S	3:35:14.57	−35:14:04.6	19.94			38490		38490	74	3
CGF 9-1	S0	3:35:25.07	−35:16:09.6	17.74	50075	11.7	50154		50115	45	1
CGF 8-2	E/S0?	3:36:13.38	−35:26:04.9	19.41			21077		21077	80	3
CGF 8-4	Sc	3:36:27.47	−35:26:02.3	19.95				94531	94531	40	2
CGF 6-3	Sbc	3:36:44.44	−35:33:48.1	18.88	42022	3.7	42328	41732	42175	74	2
CGF 6-4	S/Irr?	3:36:45.15	−35:31:48.5	19.04	52034	3.1		51420	51761	77	3
CGF 6-6	Sc	3:36:48.98	−35:31:52.7	19.10			41898	41676	41787	62	3
CGF 6-2	Sc	3:36:56.93	−35:28:21.4	18.51	50228	5.6	50105	50380	50186	44	1
CGF 6-8	Sb(LSB?)	3:37:00.58	−35:32:12.5	19.97	18539	2.6	19523		19031	67	4
CGF 6-1	Sc	3:37:01.46	−35:33:58.9	18.21	34794	6.1	34826	34729	34794	58	3
FCC 188	dE, N	3:37:04.44	−35:35:19.3	16.10	945	5.1			945	67	3
CGF 3-9	S(B)a?	3:38:01.97	−35:32:37.5	18.91	33656	10.1	33549		33594	47	1
CGF 4-3	S	3:38:05.25	−35:22:39.4	18.88			46324		46324	78	4
CGF 3-5	E	3:38:05.98	−35:32:19.1	18.05	33731	11.2	33760		33745	37	1
CGF 4-1	dEN	3:38:06.54	−35:26:24.4	14.88	868	8.0	918		882	39	1
CGF 3-7	Sb	3:38:06.58	−35:29:08.9	18.52	21933	6.4	21744	21726	21835	29	1
CGF 4-4	E	3:38:09.43	−35:25:43.0	18.92	40754	3.7	40696	40740	40714	60	2
CGF 4-6a	S	3:38:15.02	−35:27:33.5	19.16	52835	2.8	52958	53006	52939	111	3
CGF 4-6b	S	3:38:15.02	−35:27:33.5	19.16			28376		28376	94	3
CGF 3-13a	Sc(pec)	3:38:16.61	−35:30:11.0	19.48			55208	54834	55021	98	3
CGF 3-13b	Sc(pec)	3:38:16.61	−35:30:11.0	19.48			38944		38938	79	4
CGF 4-8	Sb?	3:38:17.78	−35:26:43.7	19.95	33569	4.4	33492		33531	52	2
CGF 3-2	dEN	3:38:18.71	−35:31:52.1	17.21	1625	4.4	1691		1694	85	1
CGF 3-11	S?	3:38:21.30	−35:28:50.3	19.05				52788	52788	85	4
CGF 3-6	Sa	3:38:21.79	−35:32:58.0	18.33	61415	7.4	61348		61365	53	1
CGF 3-12	Sc?	3:38:23.07	−35:28:07.2	19.27	34219	4.3	34113	34455	34225	70	1
CGF 4-2	Sa	3:38:23.49	−35:24:06.4	17.46	33946	8.8	33953		33964	62	1
CGF 3-4	ring?	3:38:25.83	−35:33:28.4	17.95	54689	8.8	54797	54663	54738	57	1
CGF 1-11	S0	3:38:28.89	−35:28:24.6	18.74	33886	10.9	33716		33785	40	1
CGF 1-1	E(cD)	3:38:29.16	−35:28:08.6	16.28	33440	18.1	33299		33355	44	1
CGF 2-3	E/S0	3:38:32.17	−35:24:30.2	18.35	33718	18.9	33509		33608	46	1
CGF 1-15	E	3:38:32.96	−35:30:12.4	19.09	36893		37047		36970	72	2
CGF 1-16	S0	3:38:35.16	−35:27:40.7	19.11	33583	7.7	33280		33412	48	1
CGF 1-18	Sb	3:38:35.93	−35:31:13.5	19.16			48747	48861	48804	72	3
CGF 2-9	Sbc	3:38:40.58	−35:20:24.5	19.16	33804	4.4	33875	33702	33840	62	2
CGF 1-9	S0?	3:38:40.93	−35:27:26.7	18.48	34321	6.4	34360	34138	34341	65	1
CGF 1-12	Sa?	3:38:41.61	−35:27:25.1	18.83	34257	7.6	34391	34194	34324	49	1
CGF 1-3	Sbc	3:38:44.75	−35:27:01.3	17.48	33143	6.8	33224	33157	33187	55	1
CGF 1-14	S0	3:38:45.47	−35:29:53.9	19.08	33354	11.3	33156		33255	34	1
CGF 2-2	E(pec)	3:38:45.97	−35:22:52.3	17.82	33798	8.9	33964	33785	33869	58	1
CGF 2-18	E	3:38:46.15	−35:22:35.2	19.91	84708	4.3	84758		84748	55	3
CGF 2-17	Irr(LSB)	3:38:46.44	−35:20:55.9	19.82	26504	3.3	25721	26422	26092	83	3
CGF 1-21	E/S0	3:38:48.20	−35:33:18.9	19.61	64630	7.4	64358		64470	56	1
CGF 1-13	Sc	3:38:49.07	−35:33:44.1	18.97			44316	44218	44267	105	3
CGF 2-6	S0/E	3:38:49.10	−35:25:30.3	18.62	33726	5.2	33675	33471	33675	65	1
CGF 1-22	S/Irr?	3:38:49.21	−35:29:19.6	19.74	82506	2.2		82343	82435	168	4
CGF 1-17	E	3:38:50.31	−35:30:56.9	19.14	73578	9.3	73590		73584	56	1
CGF 2-15	E(pec?)	3:38:51.19	−35:22:15.8	19.55	73917	8.2	73894	74159	73889	54	1
CGF 2-14	E/S0	3:38:51.50	−35:24:22.2	19.48	34341	4.1	33874		34097	60	3
CGF 2-8	Sb(pec?)	3:38:51.76	−35:22:18.0	18.97	84930	5.9	84749	84587	84809	85	2
CGF 2-16	Irr	3:38:53.08	−35:24:48.7	19.80				33540	33540	88	4
CGF 1-4	cE/GC?	3:38:54.05	−35:33:33.9	17.87	1523	23.9	1457		1485	38	1
CGF 1-19	E	3:38:54.48	−35:27:55.9	19.55	73372	4.3	73461		73431	62	3

Table 2. continued

Object Id.	Type	RA(2000)	Dec(2000)	V	$v_{\rm cross}$	R	$v_{\rm rvid}$	$v_{\rm em}$	$v_{\rm helio}$	error$_v$	Q
CGF 1-7	S0/Sb?	3:38:54.70	−35:31:04.6	18.36	53478	6.6	53470	53437	53464	58	1
CGF 1-6	E	3:38:57.22	−35:32:33.8	18.34	55066	12.2	55061		55064	48	1
CGF 1-10	S0/E	3:38:59.58	−35:30:31.7	18.69	64581	6.3	64460		64469	41	1
CGF 2-7	Irr	3:39:00.98	−35:20:29.2	18.73	33639	5.1	33517	33497	33542	58	1
CGF 2-4	S0?	3:39:01.77	−35:22:56.6	18.51	58255	2.8		58030	58143	123	4
CGF 5-8	S?	3:39:07.65	−35:29:59.7	19.60	64703	4.1	65166	64403	64935	67	3
FCC 222	dE, N	3:39:13.32	−35:22:10.9	15.60	740	8.0	964		852	52	1
CGF 5-13	Irr	3:39:18.44	−35:24:00.5	20.03			75110	75374	75242	89	2
CGF 5-7	Sa	3:39:18.61	−35:27:42.9	19.41	64349	3.9	64300		64324	67	3
CGF 5-2	E	3:39:22.44	−35:25:30.9	18.06				13904	13904	77	2
CGF 5-5	S	3:39:22.63	−35:25:29.1	19.36	26220	10.6	26261	26192	26233	57	1
CGF 5-10	E	3:39:25.66	−35:23:50.2	19.74	26355	4.6	26468		26418	69	1
CGF 5-1	S0	3:39:26.01	−35:24:14.5	17.31	26404	19.5	26339		26352	37	1
CGF 5-6	E/S0	3:39:29.37	−35:23:50.3	19.39			53106		53106	74	4
CGF 5-11	BCD?	3:39:29.60	−35:26:52.0	19.76	26342	2.8	25912	26125	26073	124	3
CGF 5-9	Sc	3:39:33.67	−35:27:06.8	19.67			26432	26099	26266	93	2
CGF 5-12	S?	3:39:33.68	−35:25:52.9	19.93	83253	3.6	83125	83095	83150	97	4
CGF 5-3	Sb	3:39:34.31	−35:27:22.0	18.48	47942	6.1	48050	47660	47996	57	1
CGF 5-4	cE/GC?	3:39:35.92	−35:28:24.9	19.05	1874	3.9	1863		1869	60	3
CGF 7-9	(d?)Irr	3:39:51.83	−35:33:05.4	19.72			1981		1981	72	4
CGF 7-10	E/S0	3:39:52.51	−35:34:46.9	19.81			73169		73169	49	4
CGF 7-8	E?	3:39:54.43	−35:38:51.7	19.72	22287	4.3	22060		22165	73	3
CGF 7-2	E	3:40:00.81	−35:35:27.7	18.62	55257	8.0	55360		55309	53	1
CGF 7-1	E(pec)	3:40:04.39	−35:36:52.6	17.16	36199	12.1	36193		36196	38	1
CGF 7-4	Sb	3:40:16.15	−35:33:14.2	19.03	36360	4.4	36404	36202	36382	72	1
CGF 7-7	E	3:40:20.04	−35:38:27.6	19.44	96894	5.3	96945		96920	57	2
CGF 10-9	E	3:42:00.93	−35:25:43.7	19.42	46416	4.4	46653		46534	77	3
CGF 10-6	Sc(BCD?)	3:42:02.09	−35:23:45.8	18.85	25725	3.3	25521	25612	25591	107	3
CGF 10-3	Sa	3:42:03.83	−35:26:47.3	18.41	54727	6.7	54714		54721	41	1
CGF 10-2	E	3:42:05.42	−35:23:58.1	17.90	57092	13.0	57095		57094	41	1
CGF 10-4	S0	3:42:06.13	−35:23:41.4	18.65	56663	4.8	56004	56632	56318	71	1
CGF 10-8	Sb?	3:42:14.75	−35:26:17.4	19.35			55053	55012	55033	123	1
FCC 274	dE, N	3:42:17.28	−35:32:20.8	16.50	1095	4.5	1058		1073	76	3
CGF 10-1	Sb?	3:42:19.01	−35:23:47.2	16.87				16409	16409	40	2
CGF 10-15	S	3:42:20.02	−35:26:14.7	20.07			29577		29577	66	4
CGF 10-5	Sc?	3:42:27.62	−35:27:01.1	18.68				38463	38463	120	4

identified lines it was also included. Column 12 indicates the quality parameter Q of the velocity determination. Table 2 is also available in electronic form at the CDS via anonymous ftp to cdsarc.u-strasbg.fr (130.79.128.5) or via http://cdsweb.u-strasbg.fr/Abstract.html.

We defined 4 classes of quality due to the clearness and evidence of the velocity identification: (1) a clear and evident identification, both methods agree very well, (2) very probable identification, almost clear, (3) doubtful, but most probable value, and (4) very doubtful, only a try.

Table 3 summarises the statistics of quality classes divided into the following sub-samples: velocities between 700 and 2500 km s^{-1} (Fornax cluster, not including the galaxies of Table 1), velocities between 33000 and 34500 km s^{-1} (background cluster, see Sect. 5.3), and all other background galaxies.

Table 3. Statistics of the quality of velocity determinations

Q	Fornax	cluster	others	total
1	4	15	23	42
2	0	2	10	12
3	3	1	22	26
4	1	1	12	14
total	8	19	67	94

In Fig. 3 we show the selection of our sample in a $\mu_{\rm eff} - V_{\rm tot}$ diagram (see also Paper I, Figs. 3 and 7). All velocity determinations of the quality classes 1 to 3 are indicated. The limits are $V_{\rm limit} \simeq 20$ mag and $\mu_{\rm eff_{lim}} \simeq 23.5$ mag arcsec^{-2}. The velocities of the fainter galaxies are mainly based on emission line identifications. Due to the low surface brightness of most dwarf galaxies (FCC

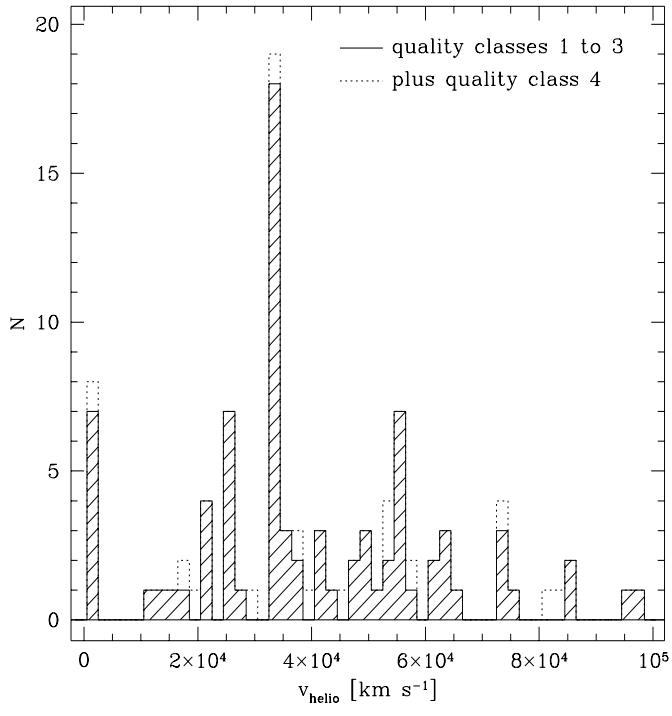

Fig. 4. Velocity histogram for all galaxies with velocity determinations. The bin size is 2000 km s^{-1} starting at 500 km s^{-1}. The concentration of galaxies at about 33700 km s^{-1} belongs to a background cluster just behind the center of the Fornax cluster

numbers) the signal-to-noise of their spectra is too low for line identifications. Among the galaxies with higher surface brightness two objects with velocities consistent with Fornax members were found.

The distribution of velocities in our sample is shown in Fig. 4. The first bin represents the Fornax cluster velocities. The highest velocity ($cz = 97000$ km s^{-1}) corresponds to a redshift of $z = 0.3$. A striking feature is the concentration of galaxies around 33700 km s^{-1} ($z = 0.11$). They belong to a background cluster behind the center of the Fornax cluster (see Sect. 5.3). Another group of galaxies with velocities around 26000 km s^{-1} is concentrated in a region about 12′ east of NGC 1399 (field B1; see Paper I). The galaxies around 55000 km s^{-1} are not spatially correlated.

5.1. Previously measured galaxies

Our velocity sample includes 12 galaxies studied before. Table 4 gives the different names, membership classifications, and previous radial velocity measurements.

Irwin et al. (1990) had no morphological classification for their targets, but noted that their compilation of low surface brightness galaxies, which they classified as members (Davies et al. 1988), might be contaminated by background galaxies in the magnitude range $17 < B < 19$ mag and of central surface brightnesses of $22.0 < \mu_B < 22.5$ mag/arcsec^2. Indeed, all galaxies in this range turn out to be background galaxies (CGF 9-1, CGF 3-6, and CGF 1-10). Concerning the FCC, all "likely background" galaxies are proved to be true background galaxies (CGF 9-1, CGF 3-7, and CGF 10-2). In addition, the likely Fornax member FCC 141 (CGF 9-5) has a velocity of $v_{\rm helio} = 16845$ km s^{-1}. Due to its blue color, $(V - I) = 0.8$ mag, it was classified as irregular. The definite FCC galaxies are confirmed to be members. Their velocities agree well with previous results.

Recently, Minniti et al. (1998) have measured radial velocities of globular clusters around NGC 1399. Their brightest object, whose nature as GC was questionned, is the same as the nucleus-like object CGF 1-4 (see next section). Their velocity of $v_{\rm helio} = 1459 \pm 52$ km s^{-1} agrees very well with our value: $v_{\rm helio} = 1485 \pm 38$ km s^{-1}.

5.2. New Fornax members

Three objects in our sample have velocities of the Fornax cluster, but have not been identified as members yet. Two of them, CGF 1-4 and CGF 5-4, are located at distances of 8.′3 and 13.′6 from NGC 1399, CGF 1-4 in the direction of NGC 1404 and CGF 5-4 in east direction. They are hardly resolved, have a circular shape, $(V - I)$ colors of 1.1 and 1.0 mag, respectively, and a very high central surface brightness. These properties are typical for globular clusters as well as for nuclei of nucleated dwarf ellipticals, or even for compact ellipticals. Adopting a distance modulus to the Fornax cluster of $(m - M)_0 = 31.3$ mag, implying a distance of 18.2 Mpc, (Kohle et al. 1996, recalibrated with new distances of Galactic GCs, Gratton et al. 1997, following Della Valle et al. 1998), their absolute magnitudes are $M_V = -13.4$ mag and $M_V = -12.2$ mag, which is about 3 magnitudes fainter than M 32 ($M_V = -16.4$ mag) and $1 - 2$ magnitudes brighter than the brightest GC of the investigated luminosity function (Kohle et al. 1996). For comparison, the brightest GCs in the central Virgo galaxy M 87 have absolute V magnitude in the order of -11.5 mag (Elson & Santiago 1996; Whitmore et al. 1995).

In order to investigate the possibility, whether these two objects might be "normal" GCs in a very rich GCS, the number of GCs that populate the bright end of the luminosity function (LF) of the GCS in NGC 1399 was estimated in Monte Carlo simulations. As representation of the LF both a Gaussian and a t5-function (see e.g. Kohle et al. 1996) with different dispersions σ were adopted. In 100 runs 5800 GCs were randomly distributed. In Table 5 the number counts in 6 bright bins (bin width 0.5 mag) are given for different functions and dispersions. Very bright GCs with $M_V = -13.3$ mag can statistically exist in a rich GCS, if the t5-function is representative for the bright wing of the LF.

According to numerical simulations by Bassino et al. (1994) nuclei of nucleated dwarf galaxies can survive the

Table 4. Cross references and comparison with velocities to previous identifications

	FCC[a]	m[b]	D&I[c]	$v_{\rm lit}$	Ref[d]	$v_{\rm helio}$[e]	Q
CGF 9-5	141	2				16833 ± 95	3
CGF 9-1	B1016	4	231			50115 ± 45	1
	188	1	76	999 ± 38	2	945 ± 67	3
CGF 4-1[f]	202	1		894 ± 120	1	882 ± 39	1
CGF 3-7	B1220	4				21835 ± 29	1
CGF 3-2	208	1	257			1694 ± 85	1
CGF 3-6			258			61365 ± 53	1
CGF 2-2				33750 ± 30	3	33869 ± 58	1
CGF 1-10			266			64469 ± 41	1
	222	1		953 ± 150	1	852 ± 52	1
CGF 10-2	B1571	4				57094 ± 41	1
	274	1	141			1073 ± 76	3

[a] Fornax Cluster Catalog (Ferguson 1989), numbers with "B" in front are from the background galaxy catalog
[b] membership classes (Ferguson 1989): 1 = definite member, 2 = likely member, 4 = likely background
[c] Davies et al. (1988) and Irwin et al. (1990)
[d] sources of radial velocities: 1 = Jones & Jones (1980), 2 = Held & Mould (1994), 3 = Carter & Malin (1983)
[e] this paper
[f] CGF 4-1 = NGC 1396.

Table 5. Number counts of GCs in the bright end of the GCLF from MC simulations. The total number of GCs is 5800. The bin centers are given in absolute V magnitudes

function	σ	−14.3 mag	−13.8 mag	−13.3 mag	−12.8 mag	−12.3 mag	−11.8 mag
t5	0.9	0.6 ± 0.8	1.2 ± 1.2	1.7 ± 1.0	2.9 ± 1.7	4.7 ± 2.2	8.8 ± 3.1
t5	1.1	1.6 ± 1.3	2.6 ± 1.5	4.2 ± 1.9	6.2 ± 2.7	10.6 ± 3.5	17.8 ± 4.1
gauss	1.2	0.0 ± 0.0	0.0 ± 0.0	0.0 ± 0.0	0.0 ± 0.0	0.5 ± 0.7	2.6 ± 1.7
gauss	1.5	0.0 ± 0.0	0.1 ± 0.3	0.6 ± 1.0	2.3 ± 1.7	5.8 ± 2.7	15.3 ± 3.2

Table 6. Line indices for Fornax members, given in magnitudes and measured on the unfluxed spectra

Galaxy	Mg2	MgH	Mgb	Fe5270	Fe5335	Hβ	Gband
NGC 1396	0.10 ± 0.02	0.02 ± 0.02	0.06 ± 0.03	0.06 ± 0.03	0.09 ± 0.03	0.07 ± 0.03	0.17 ± 0.03
FCC 188	0.13 ± 0.09	0.00 ± 0.07	0.18 ± 0.16	...	0.10 ± 0.17	0.14 ± 0.14	0.08 ± 0.17
FCC 222	0.06 ± 0.07	...	0.11 ± 0.11	0.05 ± 0.11	0.03 ± 0.13	0.06 ± 0.10	0.25 ± 0.11
CGF 1-4	0.26 ± 0.02	0.07 ± 0.02	0.17 ± 0.04	0.10 ± 0.03	0.11 ± 0.05	0.08 ± 0.04	0.17 ± 0.04
CGF 5-4	0.08 ± 0.06	0.01 ± 0.05	0.06 ± 0.11	0.10 ± 0.08	0.07 ± 0.12	0.06 ± 0.09	...

dissolution in the gravitational field of a giant elliptical over the lifetime of the universe. They expect globular-cluster-like remnants and less concentrated remnants with masses in the range between 2.8 to 7.4 10^6 $M_\odot$ and tidal radii from 170 to 400 pc.

Assuming that the two nucleus-like objects have mass-to-light ratios resembling GCs, their masses can be estimated. Adopting the relation of Mandushev et al. (1991), $\log(M/M_\odot) = -0.431\ M_V + 2.01$, we derive masses of 6.1 10^7 $M_\odot$ and 1.9 10^7 $M_\odot$ respectively. This is one order of magnitude more massive than ω Centauri (2.5 10^6 $M_\odot$), the most massive cluster in the Milky Way. Alternatively, the mass of both objects can be compared with that of M 32. Nolthenius & Ford (1986) derived a mass of about 8 10^8 $M_\odot$ and a M/L_B = 3-4 from velocity dispersion measurements. If we adopt a mass-to-light ratio of 3.5 for the two compact objects, we get masses of 6.3 10^7 $M_\odot$ and 2.1 10^7 $M_\odot$, more than one magnitude less massive than M 32.

The third object that has the velocity of the Fornax cluster, CGF 7-9, is located about 6′ north-east of NGC 1427A. Its velocity is very uncertain (Q = 4). Nevertheless, in case of membership, this galaxy belongs to the late-type dwarf population due to its blue color ($(V-I) = 0.9$) and irregular shape.

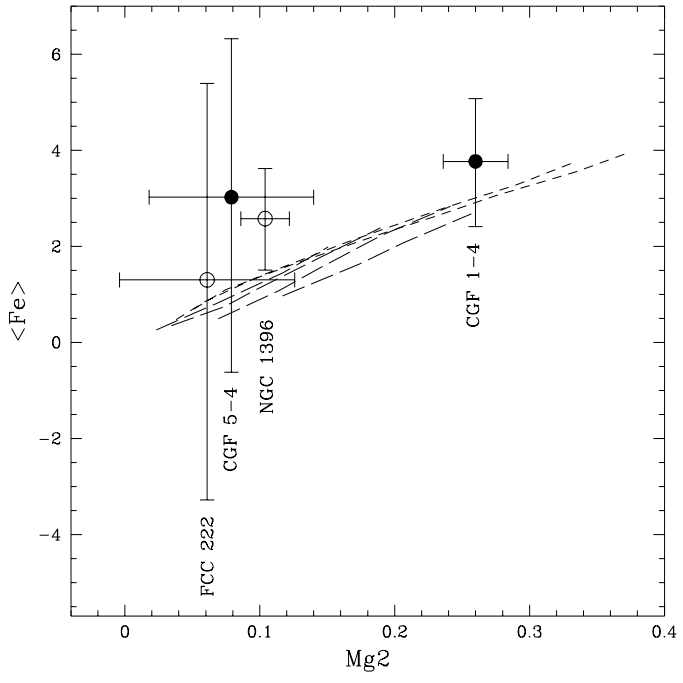

Fig. 5. Mg2 is plotted versus the equivalent width of <Fe> = (Fe5270+Fe5335)/2. The filled circles are the nucleus-like objects CGF 1-4 and CGF 5-4. Open circles are the dE, Ns FCC 122 and NGC 1396. The dashed lines are tracks from population synthesis models for single stellar populations (long dashed: Fritze-v. Alvensleben & Burkert 1995, short dashed: Worthey 1994). The age range is 1.5 to 17 Gyr, the metallicity range $-2.0 <$ [Fe/H] < 0.5 dex.

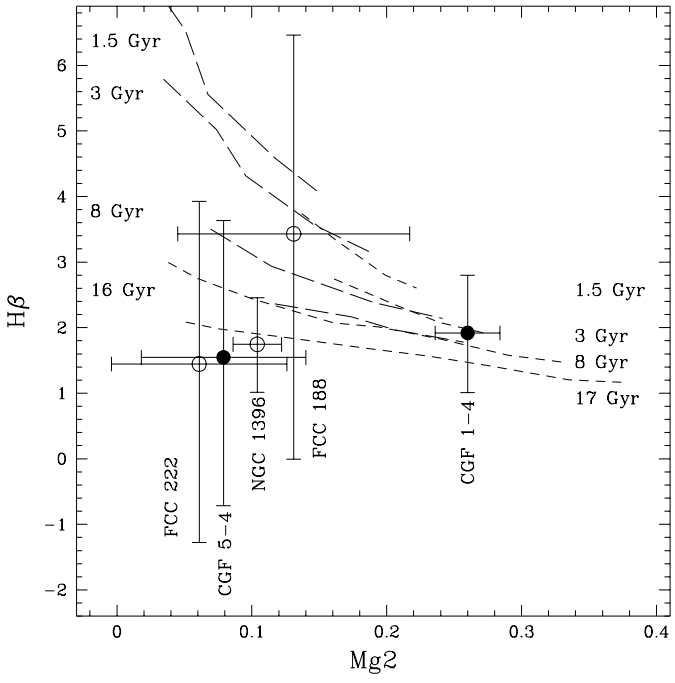

Fig. 6. Hβ versus Mg2 with tracks from Fritze-v. Alvensleben & Burkert (burk) (long dashed lines, ages on the left, metallicity between $Z = 0.001$ and $Z = 0.04$) and from Worthey (1994) (short dashed lines, ages on the right, metallicity between [Fe/H] $= -2.0$ to 0.5 dex)

5.2.1. Line indices of the Fornax members

Metal abundances of the three dE, Ns NGC 1396, FCC 188, and FCC 222 and the two nucleus-like objects were measured in order to compare them with the properties of Milky Way, LMC and NGC 1399 GCs. The procedure for the measurement of the line indices is described in Brodie & Huchra (1990). The Lick/IDS bandpasses were used, as defined by Burstein et al. (1984) and updated by Trager (1997). In Table 6 the indices, given in magnitudes and measured on the unfluxed spectra, are summarised. In the Figs. 5, 6, and 7 the line indices of Hβ, <Fe>, MgFe, and Mgb∗Fe52 are converted into equivalent widths by the relation $W_\lambda(I) = (\lambda_2 - \lambda_1)(1 - 10^{-I/2.5})$, where λ_2 and λ_1 are the maximum and minimum wavelengths of the bandpass. The errors were estimated from the photon noise in the bandpasses, $\sigma_{\rm P} = (\sigma^2_{\rm C1} + \sigma^2_{\rm L} + \sigma^2_{\rm C2})^{1/2}$, where $\sigma_{\rm L}$, $\sigma_{\rm C1}$, and $\sigma_{\rm C2}$ are the statistical errors in the line and adjacent continuum bandpasses (see Brodie & Huchra 1990). The statistical error in the flux in a bandpass is $\sigma = (O + S)^{1/2}/O$, where O and S are the total accumulated counts in the bandpass in the object and sky, respectively.

In Fig. 5 and Fig. 6 we plotted Mg2 versus the equivalent widths of <Fe> (= (Fe5270 + Fe5335)/2) and Hβ, respectively. The dE, N FCC 188 was omitted in the Mg2-<Fe> plot, since the iron lines in this spectra are too weak. Also plotted are the relations for the indices as derived from population synthesis models for single stellar populations. The long dashed lines are the models from Fritze-v. Alvensleben & Burkert (1995) for 1.5 to 16 Gyr old populations, with metallicities between $Z = 0.001$ and $Z = 0.04$. Short dashed lines are Worthey's (1994) models for 1.5 to 17 Gyr and [Fe/H] $= -2.0$ to 0.5 dex.

The larger errors (due to the low signal-to-noise of the spectra) do not allow an age separation of the objects. Notice that the nuclei of the dE, Ns and CGF 5-4 fall in the range of metal-poor old single stellar populations. Similarly, metal-poor GCs in the Milky Way and M 31 (Burstein et al. 1984; Brodie & Huchra 1990) as well as in NGC 1399 (Kissler-Patig et al. 1998) are located in this region of the plot. On the other hand, in this diagram CGF 1-4 is clearly separated from these objects and shows a more metal-rich stellar population. Its line indices are comparable to those of the metal-rich GCs in the MW, M 31, and NGC 1399 as well as the line indices of the center of M 32 (Burstein et al. 1984), which shows a slight enhancement of Hβ compared to GCs.

Adopting the Mg2−[Fe/H] relation from Brodie & Huchra (1990), the 4 more metal-poor objects have metallicities that range between [Fe/H] $\simeq -1.6$ and -0.9 dex. This agrees well with the spectroscopic measurements of 10 dE, Ns in Fornax by Held & Mould (1994).

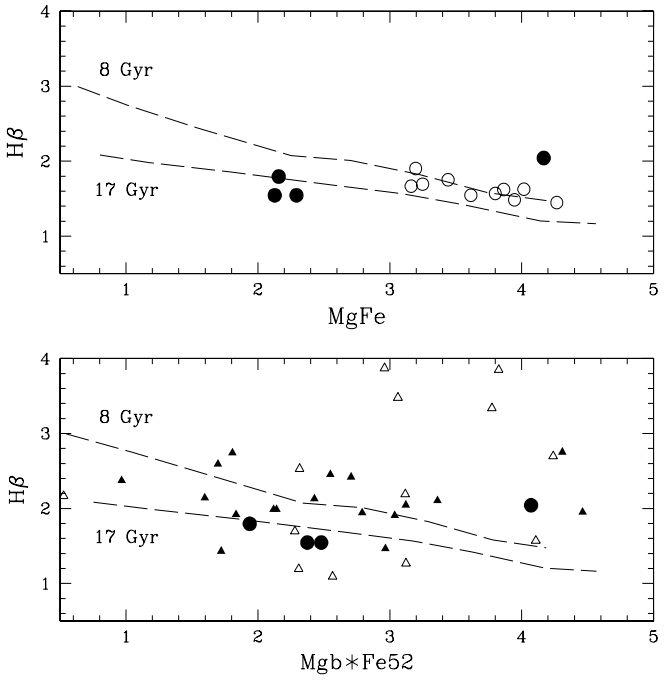

Fig. 7. [MgFe] versus Hβ for the dwarf galaxies (filled circles) and Fornax ellipticals (open circles) (upper panel), and [Mgb∗Fe52] (see text) versus Hβ for Virgo dwarf galaxies (open triangles) and NGC 1399 globular clusters (solid triangles) (lower panel). For reference, we show two models from Worthey (1994) for 17 and 8 Gyr, spanning a metallicity range [Fe/H] from −2.0 to 0.5 dex (dashed lines)

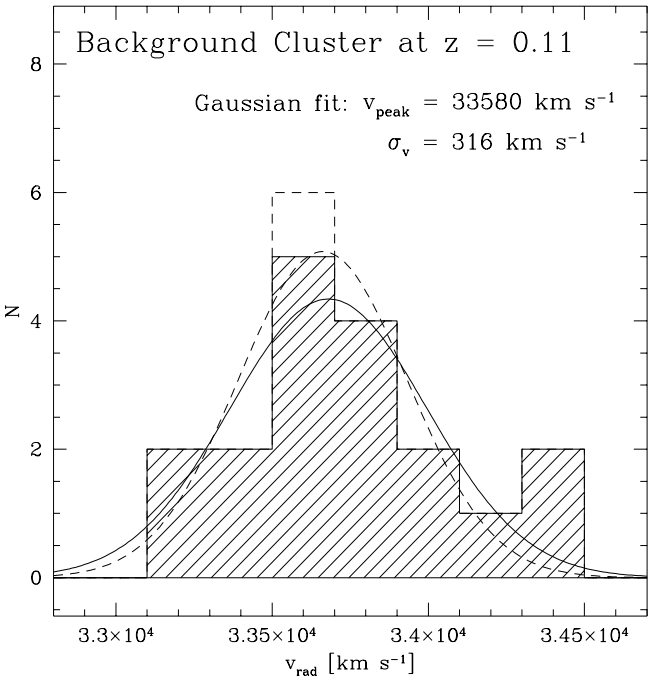

Fig. 8. Velocity histogram for background cluster galaxies. The velocity dispersion is typical for a relatively poor galaxy cluster

The metallicity of CGF 1-4 is [Fe/H] $\simeq$ 0.4 dex, when adopting the Mg2 − [Fe/H] relation by Brodie & Huchra (1990), or [Fe/H] $\simeq -0.1$ dex considering the non-linear behaviour of Mg at higher metallicities (Worthey 1994; Kissler-Patig et al. 1998).

Finally, we show in Fig. 7 a comparison between the abundances of the dwarf galaxies and elliptical galaxies in Fornax measured by Kuntschner & Davies (1998) (upper panel), as well as dwarf galaxies in Virgo (taken from Huchra et al. 1996) and globular clusters in NGC 1399 (taken from Kissler-Patig et al. 1998) (lower panel). The [MgFe] index ($\sqrt{\mathrm{Mgb}\times < \mathrm{Fe} >}$) was plotted versus H$\beta$, following Kuntschner & Davies. The Virgo dwarfs have no Fe5335 index measured. For them and the NGC 1399 GCs $\sqrt{\mathrm{Mgb} \times \mathrm{Fe5270}}$ (labeled [Mgb∗Fe52]) was plotted versus Hβ. In both panels models from Worthey (1994) for 17 and 8 Gyr, spanning a metallicity range [Fe/H] from −2.0 to 0.5 dex, are shown for reference. The large errors in our measurement prevent a detailed comparison; age differences cannot be discriminated within a factor of 2 or 3. However, we note that, as expected, the dwarf galaxies (except CGF 1-4) are less metal rich than the giant ellipticals and consistent with having similar ages. The comparison with the Virgo dwarf galaxies and the NGC 1399 GCs shows that all the Fornax dwarfs (including CGF 1-4) fall in ranges span by them. However, CGF 1-4 is more metal rich than the bulge-like GCs in NGC 1399, and could belong to the "very metal rich" group of GCs found by Kissler-Patig et al. (1998). In this case, it might also be somewhat younger, which would increase its mass-to-light ratio and reduce the estimated mass. But CGF 1-4 and CGF 5-4 remain puzzling objects; it can not yet be decided whether they are nuclei of disrupted dwarf galaxies, cEs, or true extremely massive GCs. Further spectroscopic observations with a higher signal-to-noise are needed to uncover the nature of these objects.

5.3. Background cluster at $z = 0.11$

19 galaxies with velocities around 33700 km s^{-1} (Fig. 8) were found. The velocity dispersion is about 360 km s^{-1} which is typical for poor clusters (e.g. den Hartog & Katgert 1996). The ratio of early type (E+S0) to late type (S+Irr) giant galaxies is about 1.1. It is slightly lower than in the Fornax cluster. The spatial distribution of the 19 galaxies is shown in Fig. 9 (bold hexagons). It matches well the density distribution of the fainter galaxies down to $V = 21.5$ mag; see Fig. 9 in Paper I. Since no countable amount of new Fornax dwarf galaxies was found, we conclude that the excess population of galaxies near NGC 1399 mainly belongs to the background galaxy cluster.

Assuming a Hubble constant of $H_0 = 75$ km s^{-1} Mpc^{-1} the distance to the cluster is 450 Mpc, or $(m - M)_V = 38.3$ mag. The brightest cluster galaxy (CGF 1-1), located 1′.1 south of NGC 1399,

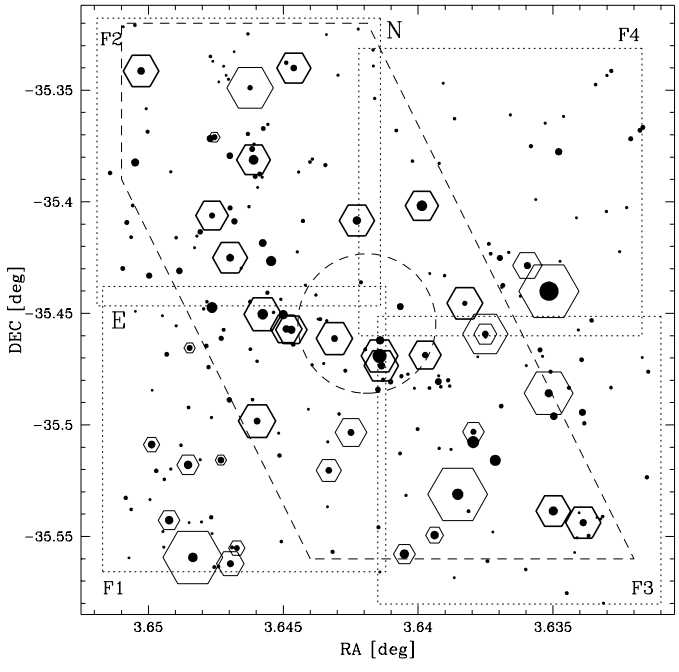

Fig. 9. Position of the background cluster galaxies in the central Fornax CCD fields. The dashed circle is the central galaxy NGC 1399. The points are galaxies brighter than $V = 21$ mag, the larger the point the brighter the galaxy. The hexagons indicate the velocities of the galaxies, the bold ones being velocities around 33700 km s^{-1}. The larger the hexagons around a galaxy the smaller is its velocity. The dashed trapezium-like region was used for the analysis of the luminosity and color distribution (see text)

would then have an absolute luminosity comparable to NGC 1399 ($M_V = -22.1$ mag). Note that the K-corrections at this redshift are in the order of 0.15 mag in V for old stellar populations and 0.05 mag for late-type spirals (Coleman et al. 1980). The radial surface brightness profile of this galaxy (see Paper I, Fig. 4) follows a de Vaucouleur profile in the inner part and becomes significantly flatter outside a radius of $7\farcs0$ ($\simeq$ 16 kpc), which is typical for a cD galaxy (e.g. Schombert 1986).

The luminosity and color distribution of the galaxies were analyzed inside a trapezium-like region that encloses the member galaxies of the background cluster (see Fig. 9). The distribution of an arbitrary sample of field galaxies around the other Fornax giant galaxies was subtracted from the distribution of the cluster galaxies.

A dip in the luminosity distribution at $V = 19.5$ was found that corresponds to an absolute magnitude of about $M_V = -18.8$ mag at a redshift of $z = 0.11$. This is the luminosity range where the Gaussian shaped giant galaxy luminosity function decreases and the counts of dwarf galaxies start to rise (see e.g. Jerjen & Tammann 1997). Of course, the dwarf galaxy counts are severely uncomplete at the cluster distance due to their very small angular diameters below our resolution limit ($1\farcs5 \simeq 3.3$ kpc). However, at the fainter counts, an excess population of blue, $(V - I) < 0.8$ mag, dwarf galaxies was found, which probably represents a population of star-forming dwarf irregulars in the cluster. Most of these galaxies are clustered around the brightest cluster galaxy (CGF 1-1) and around a bright elliptical in the north-east of the cluster (CGF 2-2).

The galaxy CGF 2-2 is already known as a narrow-line radio galaxy (Carter & Malin 1983). It is correlated with the radio source PKS 0336−35. Its spectrum shows strong O II, Ne III, and Ne V emission lines that Carter & Malin explained by a very bright high-excitation emission-line nucleus. Some of the blue faint galaxies in the direct environment of this galaxy have knots and tails. We propose that CGF 2-2 is the center of an interacting subgroup of galaxies within the background cluster.

In further investigations, this cluster might be used to constrain the amount of extinction within the central part of the Fornax cluster.

6. Summary

Radial velocities of 94 objects in central fields of the Fornax cluster have been measured with low resolution spectroscopy. Our spectroscopic sample is limited in absolute magnitude at about $V = 20.0$ mag and in peak surface brightness at about $\mu_{\rm peak} = 22.5$ mag arcsec^{-2}. Most of the velocity determinations of the fainter galaxies are based on strong emission lines of late type galaxies.

Eight objects were identified as Fornax members due to their radial velocities. Five of them are listed as nucleated dwarf ellipticals in the FCC. With one exception the membership and/or background classification by Ferguson (1989), which is based on galaxy morphology, agrees very well with our results. Among the three "new" Fornax members, there are two that have photometric properties that can be explained by a very bright GC as well as by a compact elliptical like M 32. Another explanation might be that these objects represent the nuclei of dissolved dE, Ns. The measurement of line indices has shown that the brighter one of these objects has a solar metallicity, whereas the other nucleus-like object as well as the nuclei of the measured dE, Ns have line indices that are similar to those of old metal-poor GCs. It would be interesting to investigate, whether there are more objects of this kind hidden among the high surface brightness objects in the central Fornax cluster.

Among the background galaxies we found a concentration of galaxies with velocities around $v_{\rm helio} =$ 33700 km s^{-1}. These 19 galaxies are spatially concentrated near the central Fornax galaxy NGC 1399 as well. Their velocity dispersion, $\sigma_v = 316$ km s^{-1}, is typical for a relatively poor galaxy cluster. The brightest member galaxy, located $1\farcm1$ south of NGC 1399, has a similar absolute magnitude and extended cD profile as NGC 1399.

We estimated that all excess galaxies in the central Fornax fields, except the known and "new" Fornax members, most probably belong to the background cluster just behind the Fornax center.

Acknowledgements. We thank Harald Kuntschner for providing us an electronic version of his data on elliptical galaxies in Fornax. We also thank the referee H.C. Ferguson for his useful comments which improved the paper. This research was partly supported by the DFG through the Graduiertenkolleg "The Magellanic System and other dwarf galaxies" and through grant Ri 418/5-1 and Ri 418/5-2. LI thanks Fondecyt Chile for support through "Proyeto FONDECyT 8970009".

References

Bassino L.P., Muzzio J.C., Rabolli M., 1994, ApJ 431, 634
Binggeli B., 1994, in: ESO/OHP Workshop on Dwarf Galaxies, Meylan G. & Prugniel P. (eds.). ESO, Garching
Binggeli B., Cameron L.M., 1991, A&A 252, 27
Brodie J.P., Huchra J.P., 1990, ApJ 362, 503
Burstein D., Faber S.M., Gaskell C.M., Krumm N., 1984, ApJ 287, 586
Carter D., Malin D.F., 1983, MNRAS 203, 49P
Coleman D.G., Wu C., Weedman D.W., 1980, ApJS 43, 393
Davies J.I., Phillipps S., Cawson M.G.M., Disney M.J., Kibblewhite E.J., 1988, MNRAS 232, 239
Della Valle M., Kissler-Patig M., Danziger J., Storm J., 1998, MNRAS (in press)
den Hartog R., Katgert P., 1996, MNRAS 279, 349
Drinkwater M.J., Gregg M.D., 1998, MNRAS 296, L15
Drinkwater M.J., Gregg M.D., Holman B.A., 1997, in ASP Conf. Ser. 116, Proceedings of the Second Stromlo Symposium "The Nature of Elliptical Galaxies", Arnaboldi M., Da Costa G.S. & Saha P. (eds.)
Elson R.A.W., Santiago B.X., 1996, MNRAS 278, 617
Faber S.M., 1973, ApJ 179, 423
Ferguson H.C., 1989, AJ 98, 367
Ferguson H.C., Binggeli B., 1994, A&AR 6, 67
Fritze-v. Alvensleben U., Burkert A., 1995, A&A 300, 58
Gratton R.G., Fusi Pecci F., Carretta E., Clementini G., Corsi C.E., Lattanzi M.G., 1997, in: Proceedings of the "Hipparcos Venice'97 Symposium", ESA SP-402
Held E.V., Mould J.R., 1994, AJ 107, 1307
Hilker M., Kissler-Patig M., Richtler T., Infante L., 1998, A&AS (Paper I)
Huchra J.P., Brodie J.P., Caldwell N., Christian C., Schommer R., 1996, ApJS 102, 29
Irwin M.J., Davies J.I., Disney M.J., Phillipps S., 1990, MNRAS 245, 289
Jerjen H., Tammann, G.A., 1997, A&A 321, 713
Jones J.E., Jones B.T., 1980, MNRAS 191, 685
Kennicutt Jr. R.C., 1992, ApJS 79, 255
Kissler-Patig M., Brodie P.B., Schroder L.L., Forbes D.A., Grillmair C.J., Huchra J.A., 1998, AJ 115, 105
Kohle S., Kissler-Patig M., Hilker M., Richtler T., Infante L., Quintana H., 1996, A&A 309, L39
Kuntschner H., Davies R.L., 1998, MNRAS 295, L29
Lauberts A., 1982, The ESO/Uppsala Survey of the ESO(B) Atlas. ESO, Garching
Mandushev G., Spassova N., Staneva A., 1991, A&A 252, 94
Minniti D., Kissler-Patig M., Goudfrooij P., Meylan G., 1998, AJ 115, 121
Nieto J.-L., Prugniel P., 1987, A&A 186, 30
Nolthenius R., Ford H., 1986, ApJ 305, 600
Richter O.-G., Sadler E.M., 1985, A&AS 59, 433
Schombert J.M., 1986, ApJS 60, 603
Shectman S., Carnegie Institution of Washington Year Book 1989, p. 25-32
Trager S.C., 1997, PhD Thesis, Lick Observatory
Way M.J., Quintana H., Infante L., 1998, AJ (in press)
Whitmore B.C., Sparks W.B., Lucas R.A., Macchetto F.D., Biretta J.A., 1995, ApJ 454, L73
Worthey G., 1994, ApJS 95, 107